Evaluation of microstructure properties and characterization of fracture locus of AA5083 through equal channel angular pressing techniques

Nagendra Singh 1*, , Manoj Kumar Agrawal 2

1 Research Scholar Department of Mechanical Engineering, GLA University,

Mathura, UP, India-281406

2 Associate Professor Department of Mechanical Engineering, GLA University,

Mathura, UP, India-281406

Abstract

In this investigation, a commercially available aluminium alloy called AA5083 was subjected to two passes of equal channel angular pressing utilising a route B_C at room temperature for this experiment. To evaluate the effect of AA5083, the microstructure, mechanical attributes, and wear parameters of the alloy were examined both prior to and subsequent to undergoing this technique. Using an optical microscope, microstructural investigations were performed on the pressed alloy's flow and transverse planes. The microstructure of the alloy, which had previously been coarse, had significantly improved, according to the data. As more passes were made, the alloy's microhardness and tensile strength increased simultaneously. The alloy's wear qualities were significantly improved by the equal channel angular pressing technique, which also resulted in increase in hardness and tensile strength. It is possible that a material's ductility during tensile testing does not fully reflect its capacity for plastic deformation. This study compares the state of an AA5083 alloy before and after equal channel angular pressing in order to assess the effects of the technique. The Hosford–Coulomb (H–C) model are used, the zone of equivalent strain to fracture was used to graph the fracture locus. Plasticity was examined using the Lode angle parameter and the stress triaxiality parameter. A robust correlation between the Lode angle parameter and the combined impacts of triaxiality and plasticity under stress in AA5083.

Keywords: *AA5083; SEM; Hardness; Optical Microscope, Fracture locus.*

INTRODUCTION

The process of ECAP results in the grain refinement of the alloy, leading to an adverse impact on its corrosion resistance property. Initially, the material properties were documented in tabular form before the implementation of the ECAP technique. The properties of the material after undergoing the ECAP technique were recorded in tabular format, and these were then compared against the initial properties of the material. This study clearly revealed that the mechanical properties of the material under cryogenic conditions are superior when compared to the other two sets of readings. This is associated with the reduction in the size of intermetallic

or secondary phase particles, which may serve as local cathodes or as sites for the start of localised attacks. In the case of these engineering materials, greater emphasis is placed on the mechanical and wear properties, and the ECAP technique serves as a significant strategy for producing materials with enhanced properties. In this investigation, an economically feasible AA5083 is subjected to the ECAP technique using route B_C to improve its strength [1]. Aluminum alloys find extensive use in the production of components for the automotive and aerospace sectors. Enhancements in the strength properties of these alloys are essential to meet the demands of contemporary operational conditions.

Microstructural refinement through severe plastic deformation techniques is considered a promising approach to enhance the strength characteristics of metallic materials. Materials subjected to severe plastic deformation technique can exhibit significantly elevated ultimate tensile strength, surpassing that achieved through standard treatments, making them highly promising for structural applications [2]. These materials typically display reduced ductility, restricting their suitability as substitutes for materials that haven't undergone SPD processing. In particular, transport systems use light and strong structural elements, but the plastic abilities of the material used determine the ability of the elements to resist catastrophic failure. Hence, numerous researchers are directing their efforts towards enhancing the overall strength properties of aluminum alloys through the application of Severe Plastic Deformation methods. Despite the plethora of existing literature on the relationship between microstructure, its production methods, and mechanical properties, there is still a demand for this knowledge. High strength and enhanced ductility in the novel AA5083 can be achieved through the simultaneous formation of nanoscale dispersoids and stacking faults. Alloy has a positive effect on its mechanical behavior, leading to exceptionally high strength with satisfactory uniform elongation shown in Fig. 1.

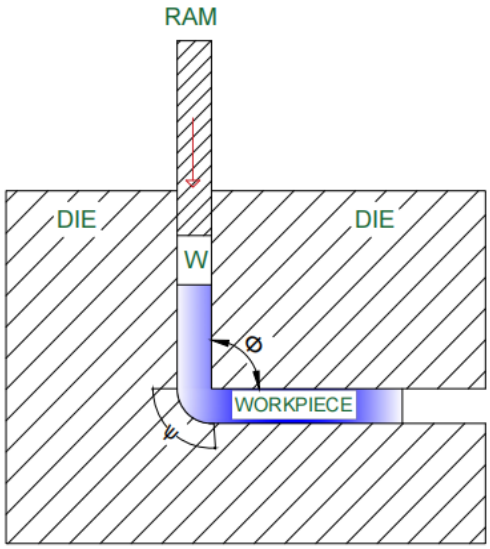

Fig. 1: The schematic sketch of ECAP process [2].

The technique involves pressing a cylindrical billet through double equal channels in a die that have an angle, where the Φ channel and Ψ corners cross section angle. The increased ductility of the annealed ultrafine grained material is attributed to the low energy dislocation configuration of geometrically necessary dislocations, a low statistically stored dislocation density and minimal grain growth. The research area is expansive and extends beyond the studies mentioned earlier. However, a commonality among all these works is the evaluation of material plasticity after SPD processing based on the results of single type tests. These tests fail to unveil the complete capabilities of these materials, especially aluminum alloys [3]. Typically, the plastic characteristics of materials before and after SPD processing are compared based on

their tensile elongation to failure, referred to as ductility. However, this method of evaluating the plasticity of materials may not always be precise. Primarily, ductility alone doesn't singularly define other plastic properties of materials, such as their capacity for processing, shaping, and forming without cracking. To validate the characteristics of materials post SPD, employing various deformation modes is imperative. Because of the unique characteristics involved in obtaining materials with a specific structure, tests are conducted on miniature specimens. The necessary utilization of non standard specimens may result in an inaccurate evaluation of the material's ductility [9]. A more comprehensive approach is required to evaluate the plasticity of materials after SPD processing through the utilization of mini specimens. This strategy must encompass diverse stress strain states that may manifest in the specimen due to distinct geometries of mini specimens arising from the limited volume of the workpiece or the methodology of specimen preparation. The literature has long discussed the substantial impact of stress states on deformation and failure mechanisms. Over the past ten years, researchers have extensively explored the impact of stress states on plastic deformation and failure by integrating damage mechanics, numerical simulations, and innovative experimental approaches. Material plasticity is commonly assessed using the equivalent plastic strain to fracture.

EXPERIMENTAL MATERIAL AND TECHNIQUE

Experimental Material

The study was carried out for AA5083. The production of construction components for shipbuilding, aviation, and mechanical engineering uses this alloy extensively. The original substance had been cast. To attain high strength and strong plasticity qualities, the structure was modified via thermomechanical processing. The processing was done using ECAP with a cross section of 10 mm diameter and 50 mm length and a channel intersection angle of 90^0. There was no backpressure used.

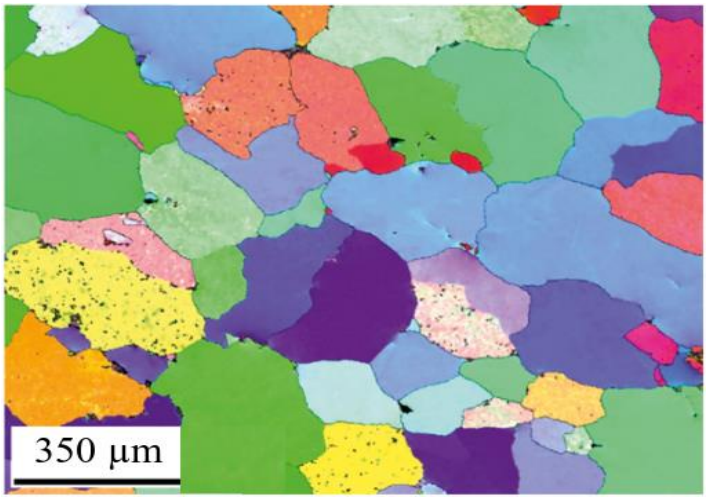

Fig. 2: Microstructure of the AA5083 in the initial state [4].

Punching occurred at 1.2 mm/min. The alloy was treated via two passes at 200 ^{0}C in total. Before the second pass at route B_C, the billets were rotated about their longitudinal axes by 90^0. The billets had the with measurements of 10 mm diameter. Through this technique, AA5083 can be made stronger without losing ductility [5]. General microstructure details of alloy before ECAP technique shown in Fig. 2. A JEOL IT-500 HR scanning electron microscope equipped with an EDAX Hikari EBSD camera was used to conduct the EBSD analysis. The EDAX OIM programme was used to calculate the EBSD maps. At an accelerating voltage of 18 kV and a step size of 0.2 m, EBSD data were collected. The goal of the data cleanup was to finish partially indexed areas that alternated between indexed and non indexed points rather than to fill in the

blank spaces on the maps. The initial material comprised equiaxed grains with no favoured orientation and an average size of 260 μm. One can see in Fig. 2 plane 3 that two cycles are insufficient to totally refine the structure because there are large patches of the same colour. Inside of huge grains, where dislocation accumulations started to rearrange, creating dislocation walls and sub boundaries with misorientations from 2^0 to 15^0, fragmentation developed.

After using the ECAP process, the material's microstructure was made up of several shear band arrays. The substance exhibited a heterogeneous structure, where some grains that appeared to be severely distorted covered regions that did not appear to be severely deformed. The predominant feature of the material was low angle grain boundaries. In planes 1 and 2, elongated grains can be seen oriented in the direction of the ECAP technique. The X-ray diffraction graphs demonstrated that the initial material had numerous secondary phase specific peaks in addition to the main Al peak and composition of material mentioned in Table 1.

Table 1: AA5083 chemical composition are showed [6].

Alloy	Si	Fe	Cu	Mn	Mg	Cr	Zn	Ti	Al
5083	0.08	0.21	0.02	0.58	1.154	0.06	<0.01	-	bal

The existence of secondary phases was, however, less prominent in the sample after the ECAP technique. Additionally, a thorough examination of the distribution of secondary phases in AA5083 was provided. A hardness profile measurement was used to assess the billet's homogeneity. A single processed piece was split in half and polished normally. The Struers Durascan 50 laboratory hardness tester was used to measure the hardness, with a normal force equal to 5.903 N and a hold period of 25 s. Three orientations were used to measure the hardness: across, perpendicular to the ECAP technique direction, and along. Steps of 1 mm were used to divide the indentations. The billet's Vickers microhardness profile after ECAP in each of its three orientations.

Experimental Technique

This is particularly relevant as the industry is increasingly interested in lightweight materials with enhanced strength but lower plasticity [6]. The majority of research focuses on fine tuning and calibrating the constitutive models used in numerical simulations, along with the formulation of optimal experimental protocols [7]. This method enables the assessment of the overall plasticity of materials subjected to the ECAP technique across a broad spectrum of stress-strain conditions, providing predictive insights into fracture during plastic deformation processes. Additionally, numerical simulations were conducted for these tests to analyze the progression of stress and strain conditions. An additional investigation of AA5083, drawing on both numerical and experimental analyses, determined that stress triaxiality has a relatively minor impact on plasticity but exerts a significant influence on ductile failure strain. Conversely, the impact of the Lode angle parameter on ductile fracture is negligible, while its influence on plasticity is noticeable. The rotation angle remains same as it passes through the first pass of a billet. After every pass along the route B_A, the rotation angle 90^0 direction changes in a different way. The workpiece turned 90^0 on even numbers of passes and 90^0 on odd numbers of passes. Every pass along the route B_C resulted in the billet rotating in the same direction 90^0, either clockwise or anticlockwise. Every pass with route C on the path always rotates 180^0 the billet shown in Fig. 3.

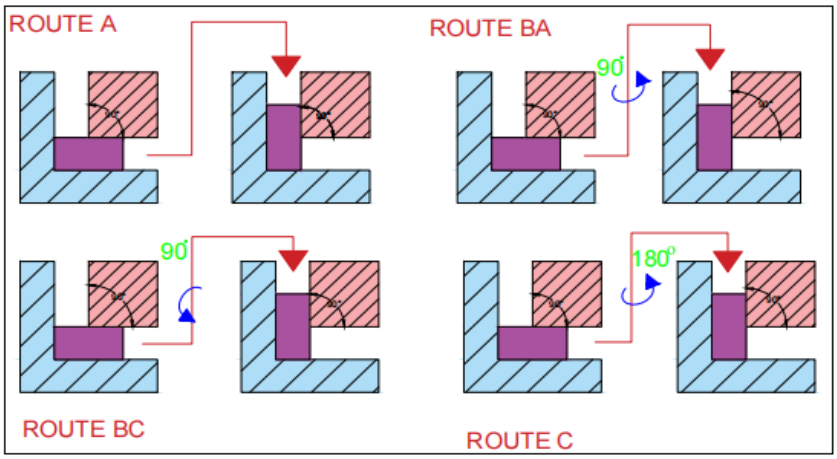

Fig. 3: Procedure for different process of ECAP technique. [8]

The emerging plasticity models generally express the equivalent plastic strain to fracture in terms of the stress triaxiality and the Lode angle parameter. A variety of tests, including uniaxial tension, plane strain tension, notched tension, shear, bending, and punch experiments, are employed to calibrate these models. Subsequently, the 3D space involving strain to fracture, triaxiality, and Lode angle parameter is identified through numerical simulation. Despite the expansion of such investigations, the utilization of a fracture locus for comparing materials and their conditions remains limited. Specifically, materials undergoing severe plastic deformation have not been explored through this methodology [8]. The fracture locus of aluminum alloys can be notably influenced by pre-strain and heat treatment. The phenomenological Hosford–Coulomb model is employed to establish the fracture locus for predicting the initiation of ductile fracture at low stress triaxialities. The fracture locus is represented in three dimensional space by the equivalent plastic strain to fracture, stress triaxiality, and Lode angle parameter. Under plain stress conditions, it is depicted as a two dimensional space involving the equivalent plastic strain to fracture and stress triaxiality.

EXPERIMENTAL RESULTS

Plasticity and Fracture Locus

Based on the measured microhardness values given in Fig. 4, an isotropic von Mises plasticity model with isotropic hardening was applied. The triaxiality, Lode angle parameter and fracture strain are the three primary parameters utilised to define the damage imparted to it. These parameters are described as stress triaxiality is expressed by Eq. (1),

$$\eta = \frac{\sigma_m}{\bar{\sigma}} \tag{1}$$

where $\bar{\sigma}$ is the corresponding von Mises stress and is the hydrostatic pressure σ_m [9]. The stress triaxiality parameter's value determines how the ductile fracture process works. In a triaxial stress field, voids can form more easily, and the magnitude of the triaxial stress has a significant impact on how quickly voids expand. This process will continue until the increasing voids merge. Greater stress concentrations result from higher levels of stress triaxiality, and failure happens at smaller strains. For the correct study of the material plasticity under the multiaxial stress, the use of the first and second stress invariants is not always sufficient, as was demonstrated. It's also important to consider the deviatoric stress tensors third invariant. Using the Lode angle parameter,

$$\theta = 1 - \frac{2}{\pi}\arccos(\xi) \tag{2}$$

where ξ is the normalized third stress invariant (J_3) [10] :

$$\xi = \frac{27J_3}{2\bar{\sigma}^3} \tag{3}$$

According to Basaran, the Lode angle parameter is the most important characteristic for AA5083 characterization. Its relevance varies according on the type of material. Additionally, when the triaxiality score increases, its significance reduces. The Lode angle parameter, which takes values of $\theta = -1$, $\theta = 0$, and $\theta = -1$ for the conditions of planar strain and axisymmetric uniaxial compression or biaxial tension, respectively, reflects the directionality of the stress state [11]. A measure of a material's ductility, equivalent strain to fracture, $\bar{\varepsilon}_f$ has a close relationship to the stress triaxiality state.

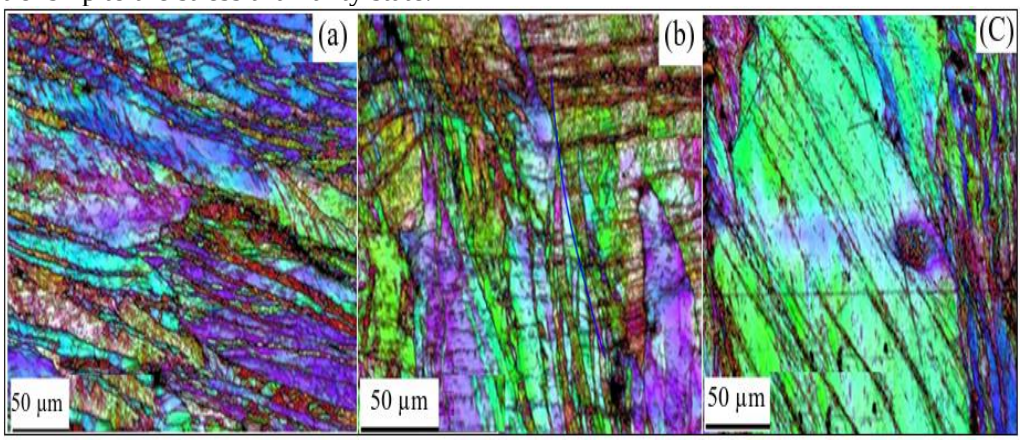

Fig. 4: IPF map shows the state the application of the ECAP technique in the three planes of the ECAP billet, with high angle bounds ($> 15^0$, red lines) and low angle boundaries ($> 2^0$, black lines) for the three fundamental plane orientations [12].

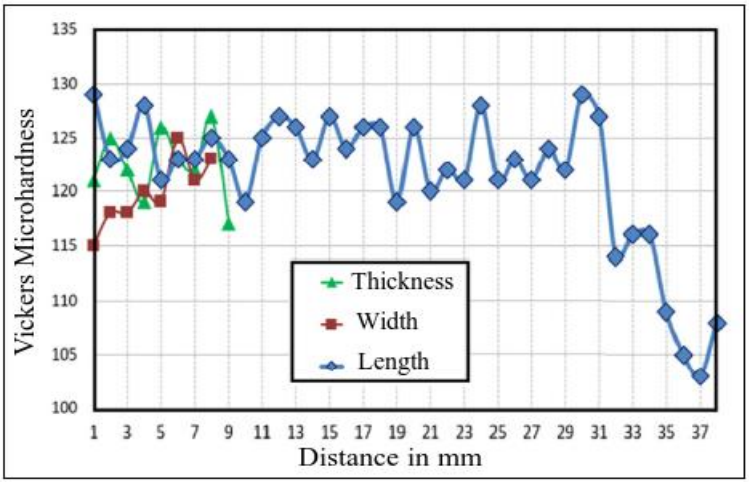

Fig. 5: ECAP technique's evaluation of the hardness values for the relevant directions and the Vickers microhardness profile measurement [13].

$$\bar{\varepsilon}_{f(\eta,\theta)} = b(1+c)^{\frac{1}{2}}\left(\left(\frac{1}{2}(f_1-f_2)^a + (f_2-f_3)^a + (f_1-f_3)^a\right)^{\frac{1}{a}} + c(2\eta + f_1 + f_3)\right)^{-\frac{1}{n}} \tag{4}$$

$$f_1 = \frac{2}{3}cos\left[\frac{\pi}{6}(1-\theta)\right] \tag{5}$$

$$f_2 = \frac{2}{3}cos\left[\frac{\pi}{6}(3+\theta)\right] \tag{6}$$

$$f_3 = -\frac{2}{3}cos\left[\frac{\pi}{6}(1+\theta)\right] \quad (7)$$

The indirect impact of deviatoric stress is controlled by exponent (a), according to Hosford. Controlling the impact of hydrostatic stress is the friction coefficient (b), which is equivalent to the friction coefficient from the Mohr-Coulomb failure criterion. The parameter (c), which is equivalent to the equivalent strain to fracture for uniaxial tension or equi-biaxial stress, affects the overall magnitude of strain to fracture. Additionally, the transformation parameter (n) is a constant [14]. As shown in Fig. 5, the fracture locus was calibrated in the present example utilising a set of miniature test specimens cut from an ECAP technique billet that covered a variety of stress-strain states.

The mini tensile test, notched tensile test, plain strain tensile test, shear test, three point bending test, and biaxial tests, specifically, were created to assess fracture stress and strain under various loading situations, spanning a wide range of triaxialities and Lode angle factors. The original state of the material was tested using the identical specimen geometries and dimensions. The cross-sectional measurements of the specimen for both material conditions. For each geometric type, a minimum of three specimens were tested. A universal electromechanical testing equipment with a load capacity of 10 kN and a maximum velocity of 1 mm/min was used to test the plane strain, shear, and tensile specimens. The specimens were modest in size, thus their strain was assessed using a virtual extensometer and a system of digital image correlation [15]. Each specimen's surface was given a stochastic pattern for the DIC evaluation, and the strain was measured using the Mercury DIC optical system, which is shown in Fig. 5. All tests were conducted with a cross head speed of 0.3 mm/min at room temperature. Using the digital camera and Pixel-fox software, the cross-sectional area of each specimen was measured after the test. Using a servo-hydraulic testing equipment with a 15 kN load capacity and a unique fixture to cause proportional biaxial loading of the test item by spherical punch, a biaxial test was carried out. The punch was a quenched ball with a 2.472 mm diameter.

The three-point bending test was run on the Mayes electromechanical universal testing apparatus, which has a load cell with a 15 kN capacity. Due to significant experimental issues with the proper application of loading, the registration of localized deformation, and the detection of the onset of failure, complete experimental results on plastic failure covering a wide range of triaxial stress states are still challenging to obtain. For test assessment, the associated plasticity was employed for simulation without damage model for a description of plastic behaviour, and Abaqus 2020 FEM software and the explicit solver were used. To speed up processing, several sample models were generated as symmetrical. The True stress-True strain dependency was used to define the material model of plasticity for the starting state and ECAP state. These curves were reconstructed using the engineering stress-strain curves that were really measured for the MTT specimen's tensile test. cross-sectional measurement of a sample inside a gauge length. For meshing the relevant specimen kinds of initial and ECAP technique material, elements of the same types and sizes were used.

The hexagonal elements used to mesh the test specimens for tensile strength were 0.15 mm in size. The element size varied throughout the specimen thickness. The finer design was also used on the other specimen types because of the smaller specimen size. Using 0.5 mm-sized hexagonal elongated elements, the shear test specimen was constructed [16]. Hexagonal components measuring 0.4 mm in size were used to mesh the planar strain specimen. The three-point bending test specimen utilised the same sort of mesh, but the element size was changed to 0.2 mm. Quadratic elements with a 0.10 mm dimension were used in the meshing of the axisymmetric specimen under biaxial loading. The specimen was constructed using CAX4R elements since the biaxial loading analysis was treated as an axisymmetric problem. The specimens were subjected to displacement-based loads. The force-displacement connection was evaluated between the data from mechanical testing and modelling. The virtual

extensometer used to calculate the displacement has contact points set up in the identical places as those for the real specimen or fixture.

EXPERIMENTAL DISCUSSIONS

Microstructure

Fig. 6 (a) and 6 (b) depict optical micrographs of the as-cast AA5083 in the transverse and flow directions. The structure of the alloy without ECAP has coarse grains. The microstructure of the billet after one pass of ECAP is depicted in Fig. 7(c) and Fig. 7 (d) depicts the specimen's microstructure after one pass along the flow direction. Due to the tremendous plastic strain produced by ECAP, it is obvious that the as-cast alloy's coarse grain structure is destroyed when it is pressed using the die. It demonstrates the material deformations caused by ECAP [17]. After two ECAP runs, the majority of the unprocessed material's coarse grain structure has been replaced with a fine and homogenous grain structure, as illustrated in Fig. 7 (c). The specimen was processed by two passes of ECAP when the micrograph in Fig. 7(d) was taken along the specimen's flow plane. It demonstrates that after two passes, the material has undergone larger deformations. The microstructure of AA5083 as-cast was improved as a result of processing by ECAP.

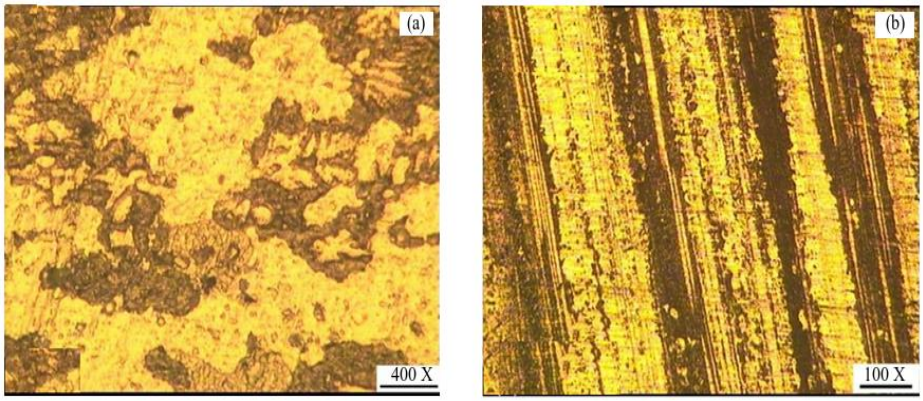

Fig. 6: Microstructure of AA5083 (a) & (b) before ECAP [18].

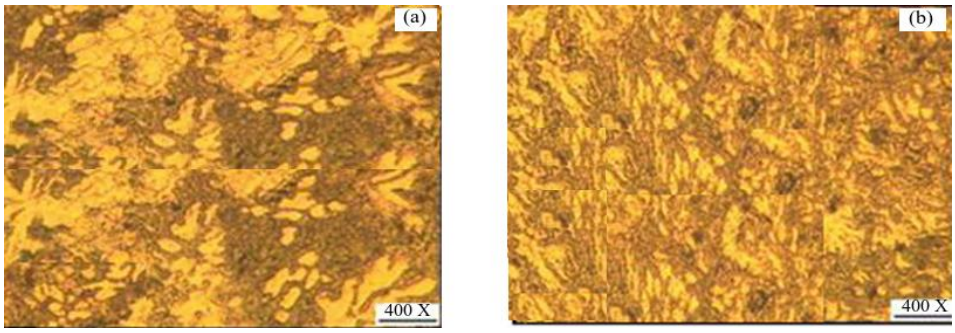

Fig. 7: Microstructure of AA5083 (c) & (d) after ECAP [19].

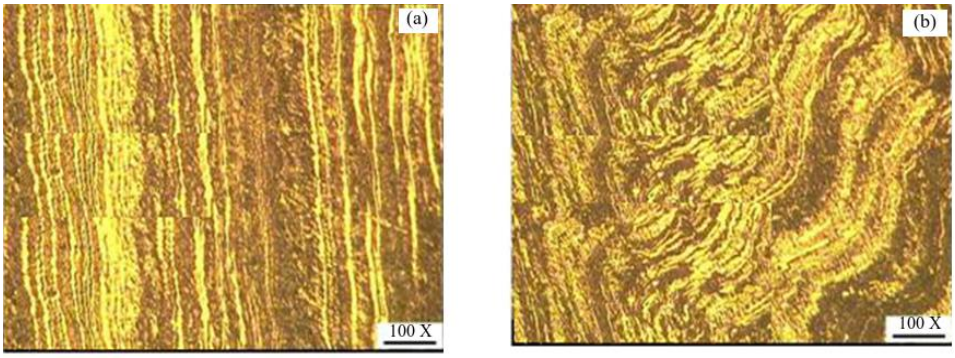

Fig. 8: (a) & (b) ECAP with cryogenic treatment [20].

Fracture Locus Characteristics of AA5083

Plasticity was taken into account as a preliminary stage. Figs. 8(a) and 8(b) compares the MTT curves for the initial and ECAPed states. The ultimate tensile strength increases from 220 MPa for the original condition to 360 MPa for the ECAPed one, demonstrating a clear strengthening effect of the ECAP technology. Additionally, 8.1% for the original condition and 8.7% for the ECAPed state showed very good agreement when the uniform elongation values were compared. However, consistent elongation is not the only indicator of ductility in a material. For the initial and ECAPed states, the second indicator of ductility decrease of area displayed values of 45% and 25%, respectively. The necking process is more obvious for the initial state, according to these results. The total elongation values, however, clearly demonstrated the opposite trend, with the ECAPed state producing a greater value of 14% in comparison to the 10% for the original condition. The current case demonstrated the opposite impact, even though the ECAP technique materials are known to have higher strength with a corresponding loss of ductility. The addition of bigger grains to a fine-grained matrix can simultaneously boost the ductility and tensile strength of AA5083. Fig. 9 makes this feature in AA5083 for ECAP technique quite evident.

The notched tensile specimen data was not used in the computation of the fracture location because of the significant fluctuation in stress data when compared to theoretical values. For MTT, NTT, and ST specimens, the DIC system, Mercury, measures major strain. Triaxiality and Lode angle parameter were these two parameters. These stress parameters were determined by numerical modelling for each specimen type. For an element where equivalent plastic strain grew most quickly, the stress parameters were assessed. Fig. 10 displays the elements that were chosen for shear and biaxial loading. Table 2 provide a summary of the stress parameters, critical strain, and weights that were determined for the various specimen types. The specimen's impact on fracture locus fitting is determined by the weight coefficient [21]. The Hosford-Coulomb model was selected for the fracture locus identification based on research. Theoretically, this failure model is applicable to specimens under tensile and biaxial loads with the same critical strain values.

By identifying the (H-C) model's (a, b and c) parameters, the fracture locus was located. Equation 4's fracture locus description is based on these input parameters. With regard to deformation and stress parameters, the goal of these parameters is to optimally interleave the fracture locus between the simulations' evaluated points. The specimen geometry, in particular the extremely precise manufacturing requirements, was the cause. The constant n was used to determine the parameter. Fig. 9 and 10 depict the mixed strain-stress space for ECAP and the consequent fracture locus in two dimensions for both material conditions. 10, notably at 0.18. Critical strain levels were almost equal between specimens loaded in shear. In particular, it was between 0.07 and 0.09 for the starting condition and the ECAP technique condition. Two specimens subjected to shear and biaxial loads were used to illustrate the effectiveness of the material model utilising identified fracture loci. The two specimens with the highest triaxiality

were chosen as references. Shear fracture predominates in the area of a stress triaxiality less than 0.2, where the equivalent strain to fracture of the material is large (Fig. 11a). According to tension mode tests, fracture brought on by pore formation predominates in the region of high stress triaxiality (Fig. 11b).

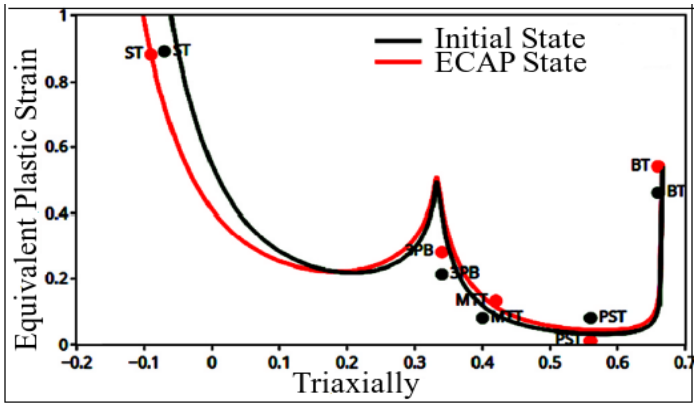

Fig. 9: Fracture locus of Hosford–Coulomb model in two Dimensional [22].

A mixed fracture regime relates to the third zone. Because the equivalent strain reduces as the stress triaxiality parameter increases, we may infer that the method of void evolution has a sizable impact on the material's flexibility. The primary forms of shear fracture are then connected to the sensitivity to the Lode angle parameter. A straightforward shear deformation criterion can be used to identify the fracture, which is caused by internal shear between voids. It is therefore reasonable to believe that the material after ECAP demonstrated a superior ability to plastic deformation during shear mode fracture than under tension mode, as compared to the material before ECAP technique. The plasticity of processed material was more adversely affected by the existence of voids and their origins. Vickers microhardness measurements utilising route- at room temperature are presented in Fig. 9 before and after ECAP. The treated alloy's hardness unexpectedly increased from 108 HV to 145 HV, and cryogenic treatment, it climbed to 154 HV. The hardness increase after one pass has a higher percentage than the two pass ECAP specimen's rise in hardness.

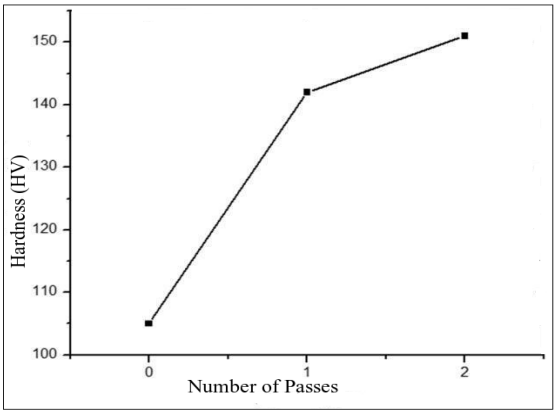

Fig. 10: Vickers hardness of AA5083 before and after ECAP [23].

Testing Properties of AA5083

Table 2 displays the tensile characteristics of AA5083 before and after ECAP. Prior to processing with ECAP, the alloy's yield strength and ultimate tensile strength were 305 MPa and 340 MPa, respectively, with a 24% elongation. The alloy's YS increased by 29% to 393 MPa after one pass of ECAP, while its UTS increased by 18% to 402 MPa with 15% elongation. In comparison to unprocessed alloy, cryogenic treatment employing ECAP to two passes raised

the alloy's YS by 43% to 437 MPa and UTS by 31% to 445 MPa with 14% elongation. Although the alloy's strength increased, its ductility dropped from 24% to 14%. However, both of AA5083's states demonstrated a substantial dependence on the stress triaxiality and Lode angle parameter together. Strong Lode angle parameter sensitivity at negative stress triaxiality and comparatively low Lode angle parameter sensitivity at high positive stress triaxiality were characteristics of the equivalent strain to fracture. From the negative to the positive range of stress triaxiality, the equivalent strain to fracture also dropped. According to the curve, the specimens for ECAP split shortly after achieving tensile strength, however in the as-cast alloy, a significant reduction in stress value is attained, which indicates the ductile type of fracture.

Table 2: Tensile properties of AA5083 before, after ECAP and after cryogenic treatment [24].

Process	Tensile Properties		
	Yield Strength	Ultimate Strength	Elongation to failure(%)
Before	305	340	24
After ECAP at room temperature	393	402	15
After Cryogenic treatment with ECAP	437	445	14

Wear Properties

Fig. 11(a) shows how load affects mass loss of both processed and unprocessed AA5083. It demonstrates that with increasing stress, the alloy's mass loss both before and after ECAP increased. When compared to extruded samples, the sample lacking ECAP exhibits a greater degree of mass loss. The maximum wear rate for the samples processed by ECAP in one and two passes is 50 N, and it decreases as the load is raised. Fig. 11(c) shows how the load affects the raw and extruded samples' friction coefficients. For the sample lacking ECAP, the friction coefficient was high and grew as the load increased. After one and two passes of ECAP with a load of 40 N, the samples' friction coefficient was initially low, reaching its maximum at a load of 50 N before decreasing further at a load of 60 N. The material's sensitivity to variations in hydrostatic stress was the same in both conditions. But the material after using the ECAP process was noticeably more sensitive to shear pressures. The example of AA5083 after ECAP demonstrated the need for a more intricate material description that takes into account multiaxial loading scenarios in order to accurately analyse the plasticity of materials for SPD. Compared to the unprocessed alloy, there is significantly less friction between the processed samples and the disc surface, resulting in significantly slower material wear for the samples. Fig. 12(a) shows the effect of sliding distance on the mass loss of the samples with and without ECAP.

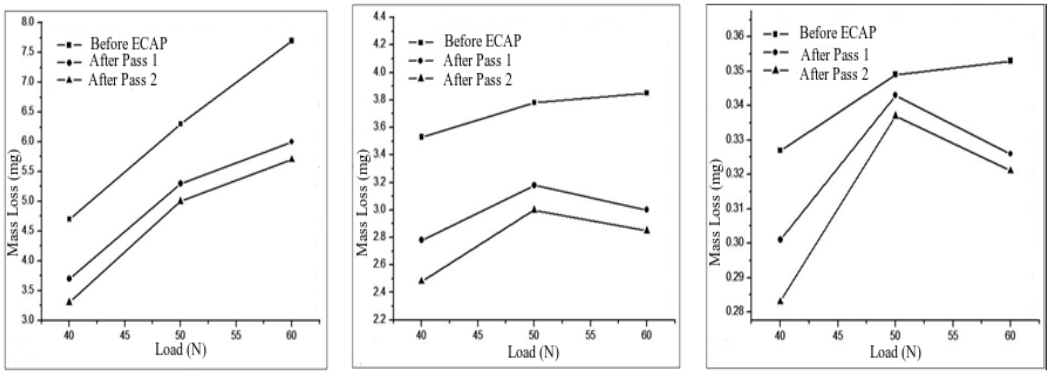

Fig. 11: Impact of load on AA5083's (a) mass loss, (b) wear rate, and (c) friction coefficient at a constant 4.19 m/s and 5 secs [25].

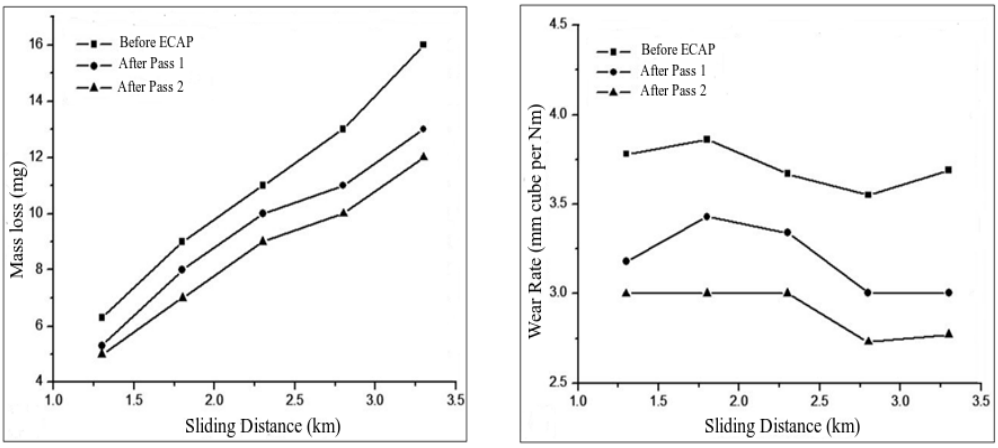

Fig. 12: Sliding distance's impact on AA5083's (a) mass loss and (b) wear rate under a constant 4.19 m/s load of 50 N [26].

The wear test reveals that the alloy's improved wear resistance has resulted from processing by ECAP with two passes. The creation and uniform dispersion of ultra fine grains are mostly to blame for this. The alloy was able to resist scratch deformation thanks to the rise in hardness that followed ECAP. Fig. 13 depicts the morphologies of the samples' worn surfaces both before and after ECAP. The specimen's worn surface before to ECAP is shown in Fig. 13(a). It is discovered that the specimen prior to ECAP has some surface delamination and an abrasive wear mechanism. The primary cause of delamination is the surface fissures created by severe plastic strain during sliding. Delamination causes some surface grooves to appear. As illustrated in Fig. 13(b), the specimen had an increase in the delamination type of wear and a decrease in the abrasive type of wear for one ECAP pass. Because flaws or defects in the material contribute in the production of cracks, the high density of dislocations imparted by ECAP increased the delamination wear. As shown in Fig. 13(c), the wear mechanism is mainly of the delamination type because of an increase in dislocation density with additional processing up to two passes. The direction of the slide is parallel to the delaminated wear particles.

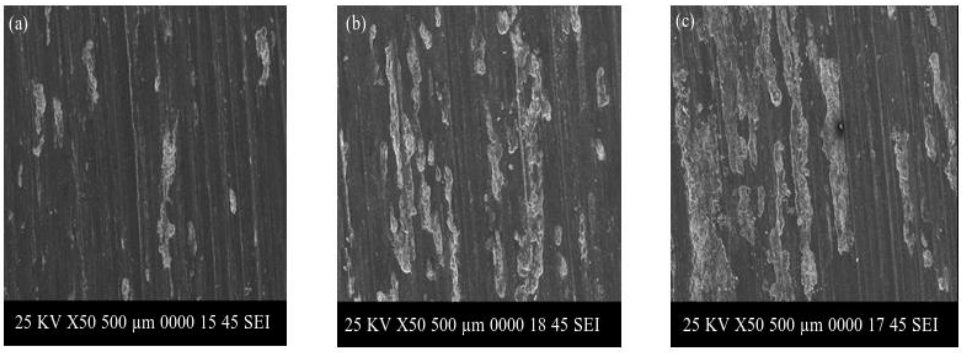

Fig. 13: Wear on AA5083's surfaces as seen using SEM morphologies: (a) without ECAP; (b) after one pass; and (c) after two passes [27].

The material's sensitivity to changes in the medium's volume under hydrostatic stress and to variations in the form of shear stresses varied between before and after ECAP processing. The material demonstrated a stronger sensitivity to shear loads after using the ECAP approach. A higher equivalent strain to failure of the material after the ECAP approach is also indicated by

parameter (b). Therefore, it may be inferred that the key H-C model parameters (a), (b), and (c) enable qualitative and quantitative comparisons of the deformation capabilities of materials before to and SPD processing. It is obvious that the stress-strain state of the aluminium alloy affects the equivalent strain to fracture. With a negative stress triaxiality, both states of AA5083 exhibit substantial Lode angle parameter sensitivity, while a high positive stress triaxiality exhibits comparatively low Lode angle parameter sensitivity. With regard to the Lode angle parameter, the fracture locus is asymmetric [28]. Additionally, the degree of the drop in the equivalent strain to fracture varies from the negative to the positive range of triaxial stress.

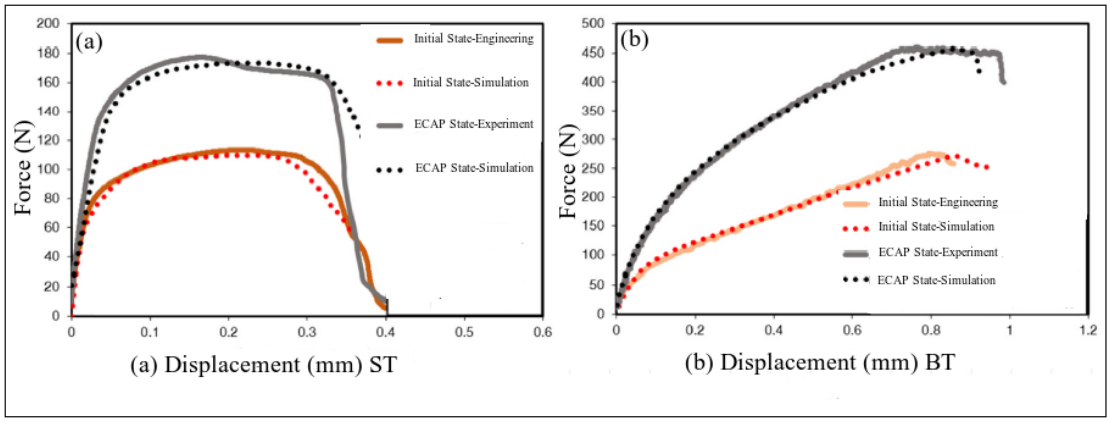

Fig. 14: Test records for ST and BT specimen, including the results of the FEM simulation tests with damage [29].

When using the ECAP approach, the material exhibits somewhat higher equivalent strain to fracture values for the range of positive triaxial stress values. The equivalent fracture strain for the starting material and the treated material when $\varepsilon = 0$ is 0.99 and 0.98, respectively. There is a difference in the little deviation of the stress triaxiality, whatever how small it is. The triaxiality for the raw material is, respectively, 0.17 and for the treated material, 0.19. Due to the mixing of grains that have been severely distorted and those that have been just slightly deformed, SPD processing not only boosted the material's strength but also gave it a somewhat higher flexibility [29]. The existence of the so-called cut-off value of stress triaxiality, a region where fracture does not occur under negative stress triaxiality. Because many metal forming processes include high compressive hydrostatic stresses, this region is of special importance. In our example, the aluminium alloy processed using the ECAP approach demonstrated a later cut-off value for stress triaxiality than the raw material. Note In contrast to aluminium 2024, the Lode angle parameter had little impact on the fracture strain of AA5083. However, only two-dimensional instances at and were regarded to fall within the stress triaxiality parameter's range of 0.6 to 1.8. In this instance, our 3D fracture surface exhibits a comparable outcome, but around 0.6, the Lode angle parameter's impact becomes discernible.

The ECAP process greatly enhanced the alloy's tensile strength while preserving its high ductility, as seen in Fig. 14(a) and 14(b). However, as can be seen from Fig. 15, the Lode angle parameter and the stress triaxiality are related to the material's plasticity deformation to fracture. This has a major bearing on the investigation of SPD processed materials. According to the Hall-Petch law, severe plastic deformation can greatly improve a material's strength by fine tuning the grain. The majority of the time, this causes the ductility failure strain at tension to drop. As a result, an understanding of the low plastic flow properties of SPD treated materials has been reached. However, the research presented here demonstrates that, depending on the stress state, the deformation before to fracture can be extremely considerable. This distinction is crucial when thinking about real constructions since in those cases, the material is used in more than just uniaxial tension loads. For metals to be used as structural materials, plastic flow is a crucial characteristic. This is a summary of the study's main conclusions and findings. After

being processed by ECAP up to two passes employing route B_C, the as-cast alloy's coarse grain structure is swapped out for a highly refined and homogenous microstructure [30]. The alloy's microhardness increased with the number of passes due to the creation of fine grains, reaching a maximum value of 154 HV after two passes. With a rise in pass number, the alloy's tensile strength also improved, however the hardening of the alloy resulted in a slight loss of ductility. After ECAP, the alloy's wear resistance rose with the least amount of mass loss and frictional coefficient.

As a result of ECAP processing, the alloy is now resistant to scratch deformation. It is evident that AA5083's mechanical and wear qualities were improved by ECAP processing. Various engineering applications needing high strength are now possible because to the alloy's improved mechanical and wear qualities. Although the structures must function under specific design loads, the original or operational stress concentrators invariably result in yielding. Due to the substitution of a strain concentration for a stress concentration, the plastic mode fails as a result. It is vital to test structural metals in complicated stress states since the stress states close to the concentrators are rarely simple, and to discern how different processing techniques affect the materials' plasticity as opposed to only their ductility. The major goal of this work was to adapt a technique for evaluating the plasticity of metals produced using SPD under various stress states. Due to the grain refinement's increased production of corrosion-initiating sites and resulting reduction in corrosion resistance, the ECAP sample's corrosion rate rose.

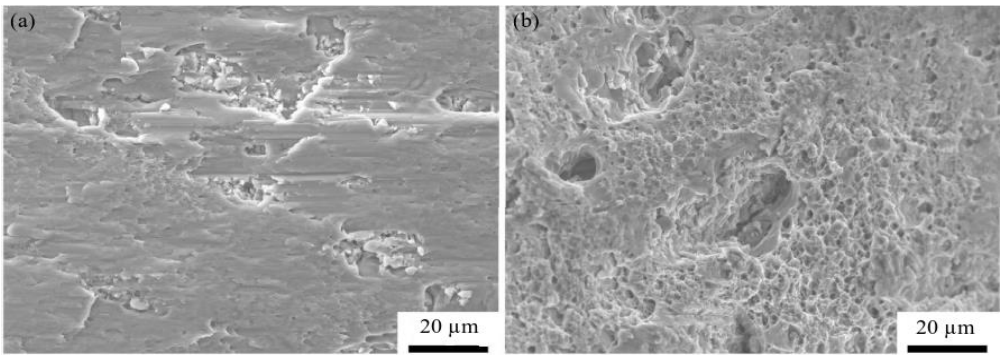

Fig. 15: Typical fracture surface of AA5053 after ECAP in various tests: a) ST; b) MTT [31].

The preliminary findings demonstrated the critical requirement for multi-axis testing of materials for SPD processing. The proposed method can be used to calculate structures formed of materials processed using the ECAP methodology as well as to identify softer mechanical processing methods, such as creating a UFG and nanocrystalline structure. However, there are still a lot of problems that require attention in subsequent work. Consideration of the these numerous ECAP technique modes and the establishment of the relationship between the microstructures parameters and the modelling parameters might be one of the first such challenges.

CONCLUSIONS

On AA5083, equal channel angular pressing was used with a suitable die design to improve the alloy's strength and wear characteristics. Using route B_C, equal channel angular pressing is applied for up to two passes, transforming the as-cast alloy's initially coarse grain structure into a highly refined and homogeneous microstructure. The alloy's microhardness showed a steady increase with each succeeding run, peaking at 154 HV after two passes. The process's creation of fine grains is responsible for this growth. After undergoing equal channel angular pressing, which is characterized by low mass loss and a low coefficient of friction, the alloy's wear resistance improved. For AA5083, the use of equal channel angular pressing produced improved wear and mechanical qualities. The plasticity properties of AA5083 were evaluated using the fracture locus in a three dimensional space defined by the stress triaxiality parameter,

Lode angle parameter, and equivalent strain to fracture, both prior to and during equal channel angular pressing. However, the mechanical properties of AA5083's two situations demonstrated a significant dependence on the combined effect of the stress triaxiality and Lode angle parameter. Under conditions of negative stress triaxiality, the equivalent strain to fracture was very sensitive to the Lode angle parameter; at high positive stress triaxiality, however, the sensitivity was comparatively smaller. Moreover, as the stress triaxiality moved from the negative to the positive range, there was a decrease in the equivalent strain to fracture. Shear fracture changed to dimple fracture in tandem with the change in stress condition.

REFERENCES

1. Frint, P.; Halle, T.; Wagner, M.F.X.; Hockauf, M.; Lampke, T. Scaling up the equal-channel angular pressing process—A study on a 6000 aluminium alloy. Mat. Sci. Eng. Tech. 2010, 41, 814–821.
2. Viceré, A.; Roventi, G.; Paoletti, C.; Cabibbo, M.; Bellezze, T. Corrosion Behavior of AA6012 Aluminum Alloy Processed by ECAP and Cryogenic Treatment. Metals 2019, 9, 408.
3. Nagendra Singh, Manoj Kumar Agrawal, Sanjeev Kumar Verma, Ashish Kumar Tiwari "Impact design of die parameters on Severe plastic deformation during Equal channel angular pressing: An overview." E3S Web of Conferences. Vol. 430. EDP Sciences, 2023.
4. Chung, M.K.; Choi, Y.S.; Kim, J.G.; Kim, Y.; Lee, J. Effect of the number of ECAP pass time on the electrochemical properties of 1050 Al alloys. Mater. Sci. Eng. A 2004, 366, 282–291.
5. Dan, S.; Jiang, J.H.; Lin, P.H.; Yang, D.H. Corrosion behavior of ultrafine-grained industrial pure Al fabricated by ECAP. Trans. Nonferr. Met. Soc. China 2011, 19, 1065–1070.
6. Brunner, J.G.; Birbilis, N.; Ralston, K.D.; Virtanen, S. Impact of ultrafine-grained microstructure on the corrosion of aluminium alloy AA2024. Corr. Sci 2012, 57, 209–2014.
7. Sun, P.L.; Kao, P.W.; Chang, C.P. Effect of deformation route on microstructural development in aluminum processed by equal channel angular extrusion, met. Mater. Trans. A 2004, 35, 1359–1368.
8. Nagendra Singh, Manoj Kumar Agrawal, Sanjeev Kumar Verma, Ashish Kumar Tiwari, A review on impact route process on AA5083 of back pressure through equal channel angular pressing, Materials Today: Proceedings, 2023.
9. Gao, L.; Cheng, X. Microstructure and mechanical properties of Cu–10%Al–4%Fe alloy produced by equal channel angular extrusion. Mater. Des. 2008, 29, 904–908.
10. Kucukomeroglu, T. Effect of equal-channel angular extrusion on mechanical and wear properties of eutectic Al–12Si alloy. Mater. Des. 2010, 31, 782–789.
11. Gao, L.L.; Cheng, X.H. Microstructure and dry sliding wear behavior of Cu 10%Al–4%Fe alloy produced by equal channel angular extrusion. Wear 2008, 265, 986–991.
12. Jiang, J.; Wang, Y.; Du, Z.; Qu, J.; Sun, Y.; Luo, S. Enhancing room temperature mechanical properties of Mg–9Al–Zn alloy by multipass equal channel angular extrusion. J. Mater. Process. Technol. 2010, 210, 751–758.
13. Ramu, G.; Bauri, R. Effect of equal channel angular pressing (ECAP) on microstructure and properties of Al–SiCp composites. Mater. Des. 2009, 30, 3554–3559.
14. Saray, O.; Purcek, G. Microstructural evolution and mechanical properties of Al–40 wt.%Zn alloy processed by equal-channel angular extrusion. J. Mater. Process. Technol. 2009, 209, 2488–2498.
15. Tolaminejad, B.; Dehghani, K. Microstructural characterization and mechanical properties of nanostructured AA1070 aluminum after equal channel angular extrusion. Mater. Des. 2012, 34, 285–292.
16. Nagendra Singh; Manoj Kumar Agrawal; Sanjeev Kumar Verma; Ashish Kumar Tiwari. "Study of the effect of ECAPed Method on the Mechanical Properties of AA 5083: An Overview". International Research Journal on Advanced Science Hub, 4, 06, 2022, 186-191.

17. Javidikia, M.; Hashemi, R. Mechanical anisotropy in ultra-fine grained aluminium tubes processed by parallel-tubular-channel angular pressing. Mater. Sci. Technol. 2017, 33, 2265–2273.
18. Mohammadtaheri, M. A new metallographic technique for revealing grain boundaries in aluminum alloys. Metallogr. Microstruct. Anal. 2012, 1, 224–226.
19. Chung, Y.H.; Park, J.W.; Lee, K.H. An analysis of accumulated deformation in the equal channel angular pressing (ECAP) process. Met. Mater. Int. 2006, 12, 289–292.
20. Gorman, J.D.; Hughes, A.E.; Jamieson, D.; Paterson, P.J.K. Oxide formation on aluminum alloys in boiling deionised water and NaCl, CeCl3 and CrCl3 solutions. Corros. Sci. 2003, 45, 1103–1124.
21. Lee, J.-C.; Seok, H.-K.; Suh, J.-Y. Microstructural evolutions of the Al strip prepared by ECAP and continuous equal channel angular pressing electrochemical behaviour. Acta Materialia 2002, 50, 4005–4019.
22. Nam, C.Y.; Han, J.H.; Chung, Y.H.; Shin, M.C. Effect of precipitates on microstructural evolution of 7050 Al alloy sheet during equal channel angular pressing effect in corrosion. Mater. Sci. Eng. A 2003, 347, 253–257.
23. Kubásek, J.; Dvorský, D.; Cˇ avojský, M.; Vojteˇch, D.; Beronská, N.; Fousová, M. Superior properties of Mg–4Y–3RE–Zr alloy prepared by powder metallurgy. J. Mater. Sci. Technol. 2017, 33, 652–660.
24. Singh, Nagendra, Dr. Manoj Kumar Agrawal, Sanjeev Kumar Verma, and Ashish Kumar Tiwari. "A Review on Effect of Stress and Strain Distribution on the AA5083 With Respect to Different Channel Angle of ECAP." International Research Journal on Advanced Science Hub 04.03 March (2022): 57–66.
25. Shuzhen, Z.; Lining, X.; Juanjuan, D.; Wei, C.; Minxu, L. Influence of acetic acid on top localized corrosion of x70 steel pipeline in CO2 containing wet gas. J. Chin. Soc. Corros. Prot. 2016, 36, 231–237.
26. Farelas, F.; Ramirez, A. Carbon dioxide corrosion inhibition of carbon steels Through bisimidazoline and imidazoline compounds studied by EIS. Int. J. Electrochem. Sci. 2010, 5, 797–814.
27. Y.W. Tham, M.W. Fu, H.H. Hng, M.S. Yong, and K.B. Lim, Bulk nanostructured processing of aluminum alloy, J. Mater. Process. Technol. 192– 193(2007), pp.575-581.
28. G. Purcek, Improvement of mechanical properties for Zn–Al alloys using equal-channel angular pressing, J. Mater. Process. Technol. 169(2005), pp.242-248.
29. A.V. Nagasekhar, Y. Tick Hon, and H.P.Seow, Deformation behavior and strain homogeneity in equal channel angular extrusion/pressing, J. Mater. Process. Technol. 192-193(2007), pp.449-452.
30. J.W. Park and J.Y. Suh, Effect of Die Shape on the Deformation Behavior in Equal-Channel Angular Pressing, Met. Mater. Trans. A 32A(2001), pp.3007-3014.
31. Radu Comaneci and Adrian Comanici, Influence of die design and process parameters on working load and damage during equal channel angular pressing, Metal, Brno, 2011.